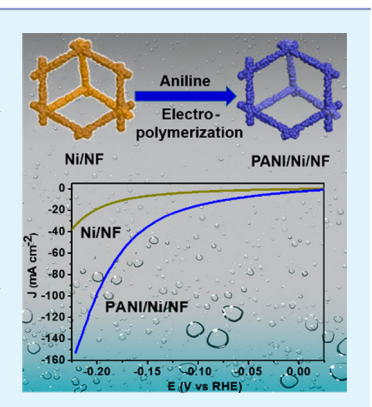
Electropolymerization of Aniline on Nickel-Based Electrocatalysts Substantially Enhances Their Performance for Hydrogen Evolution

Fuzhan Song, Wei Li, Guanqun Han, and Yujie Sun*

Department of Chemistry and Biochemistry, Utah State University, Logan, Utah 84322, United States

Supporting Information

ABSTRACT: Extensive efforts have been devoted to developing competent electrocatalysts for hydrogen evolution reaction (HER). However, limited attention has been devoted to exploring the benefits of conductive polymers to improve the performance of various HER electrocatalysts. Herein, we demonstrate that electropolymerization of aniline on nickel foam (PANI/Ni/NF) dramatically increases the latter's HER performance from pH 14 to 0. For instance, in alkaline electrolyte, PANI/Ni/NF achieved the current density of -10 mA cm⁻² at an overpotential of merely 72 mV, \sim 100 mV less than that of the pristine nickel foam. We further demonstrate that such a layer can also boost the HER performance of nickel phosphides and sulfides, highlighting the great versatility of PANI in improving the HER activities of various low-cost electrocatalysts.



KEYWORDS: electropolymerization, polyaniline, hydrogen evolution reaction, nickel electrocatalysts, hybrid composite

he concerns for increasing energy demands and climate change resulting from fossil fuel utilization have motivated the advance of conversion and storage techniques targeting clean and sustainable energy sources. ¹⁻³ Within this context, electrocatalytic hydrogen $(\overset{\smile}{H}_2)$ production from water driven by renewable energy inputs (e.g., solar and wind) stands out as an attractive option, as H2 is not only a clean fuel but also a green energy carrier with many industrial applications. 4,5 Owing to the nature of multiproton/electron arrangement of the H₂ evolution reaction (HER), its slow kinetics necessitates the development of efficient and competent electrocatalysts to achieve appreciable catalytic current density for practical applications. The state-of-the-art HER electrocatalysts are mainly those composed of platinum group elements, whose scarcity and high cost significantly hinder their large-scale commercialization.^{6,7} Recently, considerable research efforts have been devoted to developing noble metal-free HER electrocatalysts, such as transition metal sulfides, ^{8,9} selenides, ^{10,11} phosphides, ^{12,13} nitrides, ¹⁴ and carbides. ¹⁵ Nevertheless, most of them either require sophisticated synthesis or suffer from mediocre performance. It remains imperative to develop a facile and versatile approach to substantially improve the HER performance of low-cost electrocatalysts under various

Because of its large surface area and controllable hydrophilic nature, polyaniline (PANI) has attracted great attention in many electrochemical and photochemical fields, such as supercapacitance and photocatalysis. It is known that electrocatalysis is primarily occurring on the catalyst surface; hence, it is natural to modulate the surface active sites of a HER electrocatalyst to boost its performance through the means of facet tuning, heteroatom doping, and introduction of Lewis

acidic or basic sites. 18,19 Recently, PANI was reported to improve the HER performance of Co(OH)₂ nanosheets under alkaline condition, which was due to the synergistic effect between the PANI layer and Co(OH)2. 20 Nevertheless, it remained unclear whether such electropolymerization of aniline on electrocatalysts could be a versatile approach toward various electrocatalyst candidates under different conditions, such as from strong alkaline electrolytes to strong acidic media. Furthermore, compared with $Co(OH)_2$, nickel and its compounds including nickel sulfides and nickel phosphides have been reported with inherently much better HER performance. 9,13,21-24 Therefore, we were wondering whether the coating of a PANI layer would also boost the HER activities of nickel-based electrocatalysts at different pHs. Herein, we investigate the electropolymerization strategy to coat various nickel-based HER electrocatalysts with PANI. The resultant PANI-covered electrocatalysts exhibit substantially improved HER performance over a wide pH range (pH 14 to 0), demonstrating the great versatility of the electropolymerization approach of aniline in advancing HER performance. Such a surface engineering approach is complementary to other common strategies for the design and development of HER electrocatalysts.

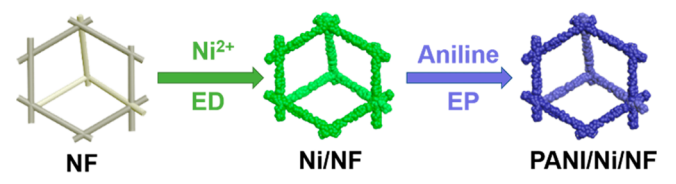
We first electrodeposited nickel nanoparticles on commercial 3D porous nickel foams (NFs) to obtain Ni/NF (see the Supporting Information for details). During the electrodeposition of nickel, the evolved $\rm H_2$ bubbles benefited the

Received: October 7, 2017 Accepted: December 4, 2017 Published: December 4, 2017



formation of porous Ni microspheres on the smooth nickel skeletons. Subsequently, electropolymerization of aniline was conducted using Ni/NF as the working electrode at a constant current density of $0.5~\text{mA}~\text{cm}^{-2}$ for 1000~s (Scheme 1) to

Scheme 1. Schematic Preparation of PANI/Ni/NF (ED, Electrodeposition; EP, Electropolymerization)



obtain the desirable PANI-coated electrodes (PANI/Ni/NF). During the electropolymerization process, the original shiny nickel foam turned to black PANI/Ni/NF (Supporting Information Figure S1). Polyaniline was also electropolymerized on fluorine-doped tin oxide (FTO) to obtain a control sample of PANI/FTO.

The X-ray diffraction (XRD) pattern of PANI/Ni/NF indicated that the surface engineering of a PANI layer on Ni/NF did not introduce new crystalline phases (Figure 1a). PANI/Ni/NF still maintained crystalline nickel as its major composition. Scanning electron microscopy (SEM) studies further confirmed the highly porous morphology of PANI/Ni/NF (Figures 1b and S2), analogous to the pristine Ni/NF (Figure S3). Many stacked nickel microspheres were decorated on the nickel foam frameworks. Figure 1c presents the elemental mapping images of Ni, C, and N in PANI/Ni/NF. The homogeneous distribution of C and N verified the successful coverage of PANI on the surface of PANI/Ni/NF. A high-resolution transmission electron microscopy (TEM) image of PANI/Ni/NF revealed the optimal thickness of the PANI layer was around 20–30 nm on the Ni/NF surface

(Figure S4). We further conducted X-ray photoelectron spectroscopy (XPS) measurement to probe the composition and valence states of elements present on the surface of PANI/Ni/NF. As shown in Figure 1d, the high-resolution N 1s spectrum could be deconvoluted into two peaks at 399.9 and 398.4 eV for the main feature, attributed to benzenoid amine and quinonoid amine, respectively. The peak at 407.1 eV was the N 1s satellite feature. The Ni 2p spectrum was plotted in Figure S5 with two peaks at 852.6 and 873.6 eV, which could be assigned to metallic Ni $2p_{3/2}$ and $2p_{1/2}$ energy levels, respectively; while the peak at 856.6 eV was due to oxidized nickel species formed during the sample preparation. Two satellite peaks of oxidized nickel species were also observed at 861.3 and 880.3 eV (Figure S5).

The as-prepared PANI/Ni/NF was directly utilized as a cathode for electrocatalytic H2 evolution in a three-electrode configuration without any other post-treatment. As comparison, Ni/NF and PANI/FTO were also evaluated for their HER performance. Figure 2a plots the linear sweep voltammograms (LSVs) of the above three electrodes assessed in 1.0 M KOH. It is apparent that the bare polyaniline layer deposited on FTO did not exhibit any HER activity within -0.225 V vs RHE (reversible hydrogen electrode), implying polyaniline itself was not an active HER electrocatalyst. In contrast, Ni/NF indeed demonstrated some activity toward electrocatalytic H2 generation, achieving current densities of -10 and -40 mA cm⁻² -0.173 and -0.225 V vs RHE, respectively. However, upon the coating of polyaniline, a much earlier catalytic takeoff and higher current density were obtained by PANI/Ni/NF. It should be noted that we optimized the electropolymerization of aniline on Ni/NF. As shown in Figures S6-S8, 1000 s electrodeposition resulted in the best HER activity. Hence, all the following PANI/Ni/NF electrodes were prepared with electropolymerization of PANI for 1000 s unless noted otherwise. The LSV of PANI/Ni/NF exhibited a catalytic current rise at a much smaller overpotential and reached -10

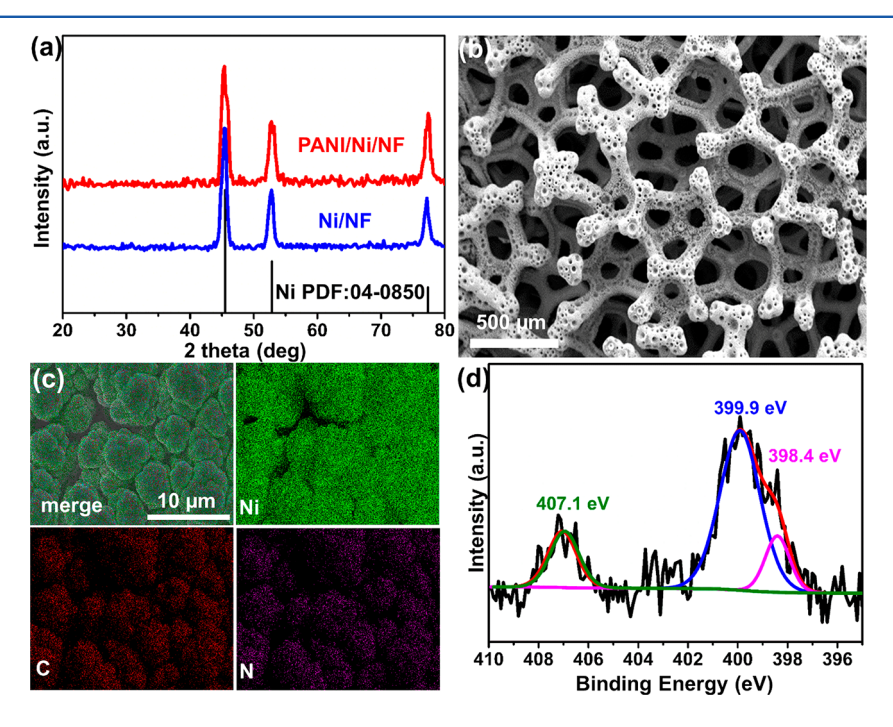


Figure 1. (a) XRD patterns of PANI/Ni/NF and Ni/NF. The standard metallic Ni XRD pattern is included for comparison. (b) SEM and (c) elemental mapping images of PANI/Ni/NF. (d) High-resolution N 1s XPS spectrum of PANI/Ni/NF.

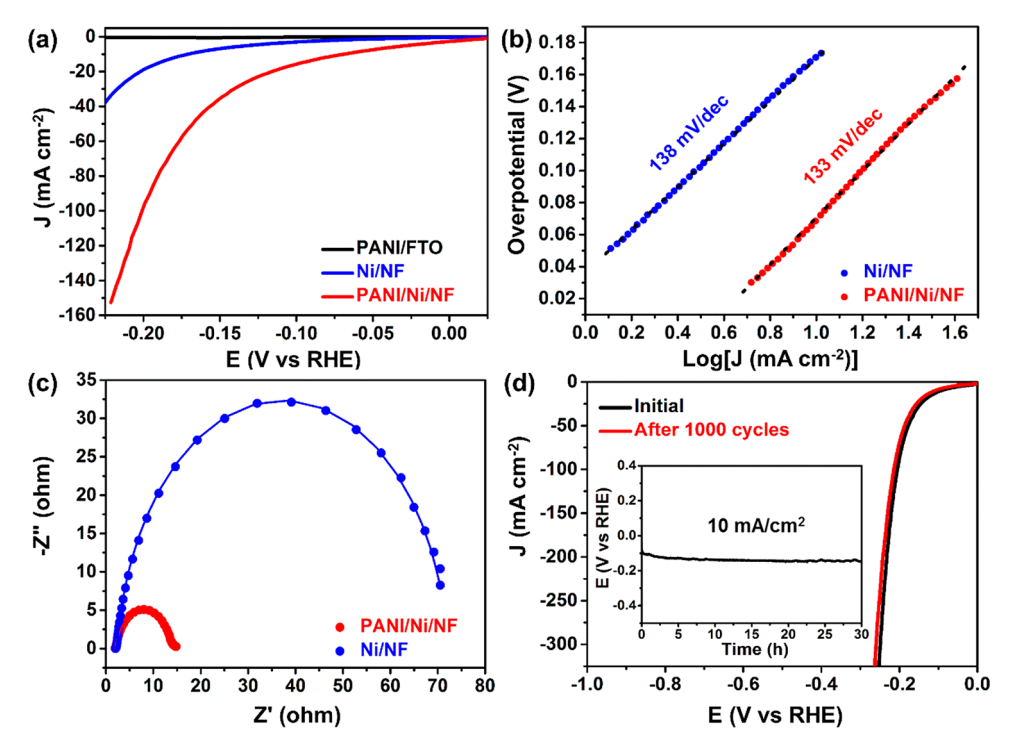


Figure 2. (a) Linear sweep voltammograms of PANI/FTO, Ni/NF, and PANI/Ni/NF at a scan rate of 5 mV s $^{-1}$. (b) Tafel plots of Ni/NF and PANI/Ni/NF with their linear fittings. (c) Nyquist plots of Ni/NF and PANI/Ni/NF measured at -0.127 V vs RHE. The data were fitted using the modified Randle equivalent circuit model shown in Figure S9. (d) Linear sweep voltammograms of PANI/Ni/NF before and after 1000 cycles at a scan rate of 100 mV s $^{-1}$. The inset shows the chronopotentiometry curve of PANI/Ni/NF conducted at -10 mA cm $^{-2}$. All of the above experiments were carried out in 1.0 M KOH.

mA cm $^{-2}$ at -0.072 V vs RHE in 1.0 M KOH, nearly 100 mV smaller than that of the parent Ni/NF (Figure 2a). Such a small overpotential requirement for -10 mA cm $^{-2}$ compares favorably with many other recently reported noble metal-free HER catalysts in 1.0 M KOH, including H $_2$ -CoCat (>385 mV), NiFe LDH (>200 mV), and Ni $_2$ P nanoparticles (221 mV). Additionally, PANI/Ni/NF produced a current density of -160 mA/cm 2 at -0.225 V vs RHE, almost four times that of Ni/NF at the same potential.

The LSV-derived Tafel plots of PANI/Ni/NF and Ni/NF are compared in Figure 2b. The Tafel slope of PANI/Ni/NF is smaller than that of Ni/NF, implying a better kinetic rate for HER. Since both of their Tafel slopes are larger than 119 mV/ dec, it suggests that water adsorption and dissociation plus the Volmer step (proton adsorption) are the rate-determining process for their HER activities. Electrical impedance spectroscopy was collected for both PANI/Ni/NF and Ni/NF at −0.127 V vs RHE in Figure 2c, and the obtained Nyquist plots are fitted with a modified Randel model (Figure S9). The charge transfer resistance (R_{ct}) at the electrode/electrolyte interface was estimated to be 68.9 and 10.5 Ω for Ni/NF and PANI/Ni/NF, respectively. The much smaller semicircular diameter of the Nyquist plot of PANI/Ni/NF relative to that of Ni/NF implies a remarkably lower charge transfer resistance of the former, which is beneficial to electrocatalytic H₂ evolution.

Given the similar composition and morphology between PANI/Ni/NF and Ni/NF, their electrochemically active surface areas (ECSAs) were also estimated from the electrochemical double-layer capacitance ($C_{\rm dl}$) measurement. As shown in Figure S10, linear plots derived from the cyclic voltammograms collected in the non-Faradaic region (0.06–0.16 V vs RHE) resulted in $C_{\rm dl}$ values of 11.1 mF cm⁻² for PANI/Ni/NF and

4.9 mF cm $^{-2}$ for Ni/NF. Since ECSA is linearly proportional to $C_{\rm dl}$ for electrocatalysts of similar composition, the nearly twice ECSA of PANI/Ni/NF compared to that of Ni/NF is in agreement with the better HER activity of the former. However, we note that the enhanced HER performance of PANI/Ni/NF should not be solely attributed to its increased ECSA, in that almost four times the current density was achieved by PANI/Ni/NF compared to Ni/NF at -0.225 V vs RHE (Figure 2a). The nitrogen groups in PANI may also function as local Lewis bases which facilitate the water adsorption/dissociation step prior to H_2 evolution on PANI/Ni/NF.

Another important factor in assessing an electrocatalyst is its long-term stability. We carried out 1000 cyclic voltammograms of PANI/Ni/NF at a scan rate of 100 mV s⁻¹ between 0 and −0.15 V vs RHE. Its linear sweep voltammograms prior to and post these 1000 cycles nearly overlapped with each other (Figure 2d). In addition, we further conducted a 30 h chronopotentiometry experiment at -10 mA cm⁻² in 1.0 M KOH. The rather stable potential evolution curve over time shown in the Figure 2d inset, together with the negligible change in LSV curves, strongly demonstrate the great robustness of PANI/Ni/NF for long-term H₂ evolution under alkaline condition. The SEM and elemental mapping images of PANI/Ni/NF collected after the long-term HER electrolysis did not present any apparent morphology and composition changes (Figures S11 and S12), further corroborating its superior robustness for extended HER electrolysis.

The excellent HER activity and stability of PANI/Ni/NF under alkaline condition prompted us to investigate its HER performance in neutral and acidic electrolytes. In particular, neutral electrolyte is the ultimately ideal condition for H₂

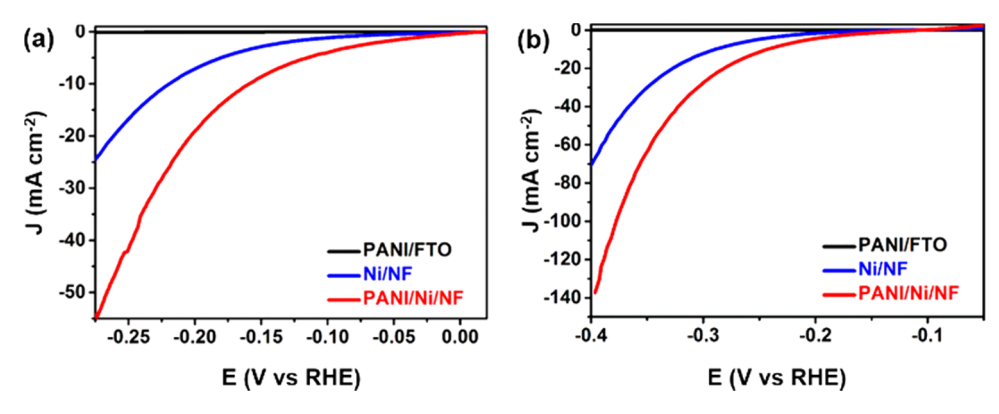


Figure 3. Linear sweep voltammograms of PANI/FTO, Ni/NF, and PANI/Ni/NF collected at a scan rate of 5 mV s⁻¹ in 1.0 M phosphate buffer at pH 7 (a) and 0.5 M H₂SO₄ at pH 0 (b).

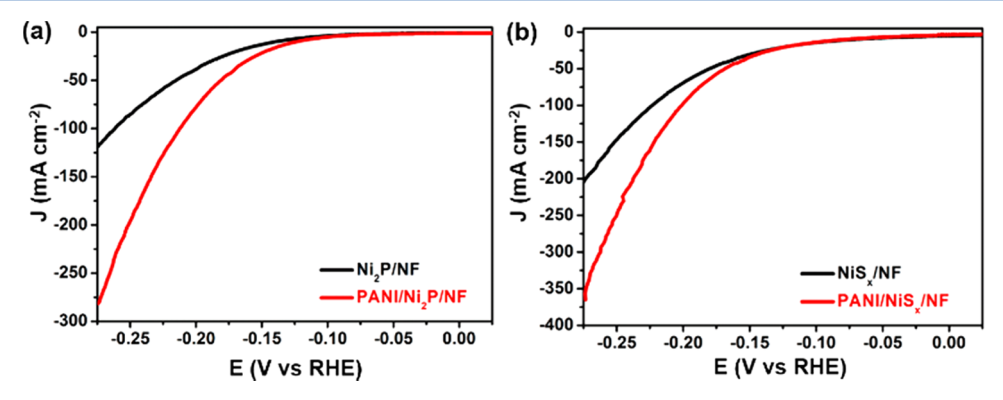


Figure 4. Linear sweep voltammograms of (a) PANI/Ni₂P/NF and Ni₂P/NF, and (b) PANI/NiS_x/NF and NiS_x/NF collected at a scan rate of 5 mV s⁻¹ in 1.0 M KOH.

evolution because of its environmental friendliness and biocompatibility. Recently, there has been rising interest in developing HER electrocatalysts for neutral conditions as these electrocatalysts can be coupled with enzymes and bacteria to assemble hybrid inorganic-biological systems for the production of biofuels and bioproducts.²⁸ However, most reported HER electrocatalysts only exhibit rather poor or mediocre performance and stability at pH 7.29 Figure 3a is a compilation of the linear sweep voltammograms of PANI/FTO, Ni/NF, and PANI/Ni/NF in 1.0 M phosphate buffer of pH 7. Analogous to the situation under alkaline condition (Figure 2a), polyamine itself was not particularly active toward HER at pH 7, showing no observable catalytic current on FTO within -0.275 V vs RHE. Ni/NF was active for HER evolution and exhibited a catalytic HER current rise beyond -0.15 V vs RHE. After the surface coating of a polyaniline layer, PANI/Ni/NF undoubtedly presented the best HER performance (Figure 3a), achieving current intensities of -10, -20, and -50 mA cm⁻² at -0.158, -0.203, and -0.266 V vs RHE, respectively, much superior to those of Ni/NF. The overpotential requirement of merely 158 mV to arrive at -10 mÅ cm⁻² at pH 7 makes PANI/Ni/NF better than many reported earth-abundant electrocatalysts for HER, such as NiS (\sim 387 mV), 30 amorphous MoS_x (>290 mV), 31 electrodeposited NiMoZn (\sim 187 mV), 32 H_2 -CoCat (>500 mV), Ni-Mo-S/C (200 mV), and h-NiS_x (210 mV). The better HER performance for PANI/Ni/ NF in comparison to that of Ni/NF was also supported by a smaller semicircular diameter in the electrochemical impedance spectroscopy of the former (Figure S13), implying lower contact and charge transfer resistance. The ESCA of PANI/Ni/ NF estimated from its cyclic voltammograms collected in a

non-Faradaic region rendered a $C_{\rm dl}$ value of 8.09 mF cm⁻², which was more than two times that of Ni/NF (3.06 mF cm⁻², Figure S14). In addition, the robust stability of PANI/Ni/NF for H_2 evolution at pH 7 was manifested by the little degradation of its LSV curves before and after 1000 consecutive CV scans between 0 and 0.5 V vs RHE (Figure S15). Long-term chronopotentiometry carried out at -10 mA cm⁻² (Figure S15 inset) further corroborated the great robustness of PANI/NI/NIE

Even more exciting was that the polyaniline layer was able to not only increase the HER activity but also stabilize nickel species in strongly acidic electrolytes (e.g., 0.5 M H₂SO₄). The LSV curves shown in Figure 3b clearly present that PANI/Ni/NF exhibited improved HER performance over those of Ni/NF and PANI/FTO in 0.5 M H₂SO₄. The results of 1000 continuous CV cycles and 30 h chronopotentiometry further demonstrated the superior robustness of PANI/Ni/NF as a HER electrocatalyst under acidic condition (Figure S16). Lower charge transfer resistance (Figure S17) was also measured for PANI/Ni/NF relative to Ni/NF in 0.5 M H₂SO₄.

Recent years have witnessed the success of various transition metal chalcogenides and pnictides for promising electrocatalytic activities for H₂ production from water. In order to evaluate the versatility of our surface engineering approach of electropolymerization of aniline, we further coated the PANI layer on nickel phosphides (PANI/Ni₂P/NF) and sulfides (PANI/NiS_x/NF). It should be noted that the surface coating of PANI did not alter the crystal structure and morphology of the resultant electrocatalysts relative to their pristine counterparts (Figures S18–S21). To our delight, the PANI layer indeed boosted the HER activities for both PANI/Ni₂P/NF and PANI/NiS_x/NF

compared with Ni₂P/NF and NiS_x/NF in 1.0 M KOH (Figure 4), highlighting the versatility and effectiveness of such a facile electropolymerization strategy in improving H₂ production.

All of the above results unambiguously prove that surface coating of a PANI layer on nickel-based HER electrocatalysts could substantially increase their electrocatalytic performance. Such an improvement could be rationalized by the following reasons: (i) the presence of nitrogen groups in PANI might speed up the water adsorption/dissociation steps before H₂ formation on nickel; ^{27,34} (ii) PANI exhibited high affinity toward various electrocatalysts, resulting in great catalyst robustness; and (iii) the coating of PANI did not change the hierarchically porous structure of those nickel-based electrocatalysts, hence substrate water and product H₂ still being able to migrate through the interconnected network freely.

In summary, we successfully demonstrated that electropolymerization of aniline on various nickel-based electrocatalysts remarkably increased their performance toward $\rm H_2$ evolution in water of a wide pH range (pH 14 to 0). The polyaniline layer coated on the electrocatalyst surface did not alter the bulk composition and conductivity of the catalyst but provided more active sites on the surface, potentially attributing to the presence of local nitrogen groups in the polyaniline layer. Its convenient surface engineering and great versatility toward other electrocatalyst candidates make us confident that this electropolymerization strategy could be widely adopted in many other electrocatalysis applications. Further efforts focusing on polymer tuning and electrocatalyst selection are currently underway in our group.

ASSOCIATED CONTENT

S Supporting Information

The Supporting Information is available free of charge on the ACS Publications website at DOI: 10.1021/acsaem.7b00005.

Details on the experimental methods, instruments, and SEM, XRD, XPS, and electrochemical measurements (PDF)

AUTHOR INFORMATION

Corresponding Author

*E-mail: yujie.sun@usu.edu.

ORCID

Wei Li: 0000-0003-2802-7443 Yujie Sun: 0000-0002-4122-6255

Notes

The authors declare no competing financial interest.

ACKNOWLEDGMENTS

This work was supported by Utah State University (USU) and the National Science Foundation (Grant CHE-1653978). We acknowledge the Microscopy Core Facility at USU.

REFERENCES

- (1) Cook, T. R.; Dogutan, D. K.; Reece, S. Y.; Surendranath, Y.; Teets, T. S.; Nocera, D. G. Solar Energy Supply and Storage for the Legacy and Nonlegacy Worlds. *Chem. Rev.* **2010**, *110*, 6474–6502.
- (2) Pan, Y.; Lin, Y.; Chen, Y. J.; Liu, Y. Q.; Liu, C. G. Cobalt Phosphide-Based Electrocatalysts: Synthesis and Phase Catalytic Activity Comparison for Hydrogen Evolution. *J. Mater. Chem. A* **2016**, *4*, 4745–4754.
- (3) Pan, Y.; Chen, Y. J.; Lin, Y.; Cui, P. X.; Sun, K. A.; Liu, Y. Q.; Liu, C. G. Cobalt Nickel Phosphide Nanoparticles Decorated Carbon

- Nanotubes as Advanced Hybrid Catalysts for Hydrogen Evolution. *J. Mater. Chem. A* **2016**, *4*, 14675–14686.
- (4) Cobo, S.; Heidkamp, J.; Jacques, P. A.; Fize, J.; Fourmond, V.; Guetaz, L.; Jousselme, B.; Ivanova, V.; Dau, H.; Palacin, S.; Fontecave, M.; Artero, V. A Janus Cobalt—Based Catalytic Material for Electro-Splitting of Water. *Nat. Mater.* **2012**, *11*, 802—807.
- (5) McCrory, C. C. L.; Jung, S.; Ferrer, I. M.; Chatman, S. M.; Peters, J. C.; Jaramillo, T. F. Benchmarking Hydrogen Evolving Reaction and Oxygen Evolving Reaction Electrocatalysts for Solar Water Splitting Devices. J. Am. Chem. Soc. 2015, 137, 4347–4357.
- (6) Jiao, Y.; Zheng, Y.; Jaroniec, M.; Qiao, S. Z. Design of Electrocatalysts for Oxygen—and Hydrogen—Involving Energy Conversion Reactions. *Chem. Soc. Rev.* **2015**, 44, 2060—2086.
- (7) Ai, L. H.; Tian, T.; Jiang, J. Ultrathin Graphene Layers Encapsulating Nickel Nanoparticles Derived Metal—Organic Frameworks for Highly Efficient Electrocatalytic Hydrogen and Oxygen Evolution Reactions. ACS Sustainable Chem. Eng. 2017, 5, 4771—4777.
- (8) Jaramillo, T. F.; Jorgensen, K. P.; Bonde, J.; Nielsen, J. H.; Horch, S.; Chorkendorff, I. I. Identification of Active Edge Sites for Electrochemical H₂ Evolution from MoS₂ Nanocatalysts. *Science* **2007**, 317, 100–102.
- (9) You, B.; Sun, Y. Hierarchically Porous Nickel Sulfide Multifunctional Superstructures. *Adv. Energy Mater.* **2016**, *6*, 1502333.
- (10) Gao, M.; Liang, J.; Zheng, Y.; Xu, Y.; Jiang, J.; Gao, Q.; Li, J.; Yu, S. An Efficient Molybdenum Disulfide/Cobalt Diselenide Hybrid Catalyst for Electrochemical Hydrogen Generation. *Nat. Commun.* **2015**, *6*, 5982.
- (11) Li, W.; Gao, X.; Xiong, D.; Wei, F.; Song, W.; Xu, J.; Liu, L. Hydrothermal Synthesis of Monolithic Co₃Se₄ Nanowire Electrodes for Oxygen Evolution and Overall Water Splitting with High Efficiency and Extraordinary Catalytic Stability. *Adv. Energy Mater.* **2017**, *7*, 1602579.
- (12) Pan, Y.; Liu, Y. Q.; Lin, Y.; Liu, C. G. Metal Doping Effect of the $M-Co_2P/Nitrogen$ Doped Carbon Nanotubes (M=Fe, Ni, Cu) Hydrogen Evolution Hybrid Catalysts. ACS Appl. Mater. Interfaces **2016**, 8, 13890–13901.
- (13) You, B.; Jiang, N.; Sheng, M.; Bhushan, M.; Sun, Y. Hierarchically Porous Urchin–Like Ni_2P Superstructures Supported on Nickel Foam as Efficient Bifunctional Electrocatalysts for Overall Water Splitting. *ACS Catal.* **2016**, *6*, 714–721.
- (14) Chen, W.; Sasaki, K.; Ma, C.; Frenkel, A. I.; Marinkovic, N.; Muckerman, J. T.; Zhu, Y.; Adzic, R. R. Hydrogen–Evolution Catalysts Based on Non–Noble Metal Nickel–Molybdenum Nitride Nanosheets. *Angew. Chem., Int. Ed.* **2012**, *51*, 6131–6135.
- (15) Vrubel, H.; Hu, X. Molybdenum Boride and Carbide Catalyze Hydrogen Evolution in Both Acidic and Basic Solutions. *Angew. Chem., Int. Ed.* **2012**, *51*, 12703–12706.
- (16) Wang, L.; Feng, X.; Ren, L.; Piao, Q.; Zhong, J.; Wang, Y.; Li, H.; Chen, Y.; Wang, B. Flexible Solid—State Supercapacitor Based on a Metal—Organic Framework Interwoven by Electrochemically—Deposited PANI. *J. Am. Chem. Soc.* **2015**, *137*, 4920—4923.
- (17) Li, X.; Wang, D.; Cheng, G.; Luo, Q.; An, J.; Wang, Y. Preparation of Polyaniline—Modified TiO₂ Nanoparticles and Their Photocatalytic Activity under Visible Light Illumination. *Appl. Catal., B* **2008**, *81*, 267–273.
- (18) Schweinberger, F. F.; Berr, M. J.; Doblinger, M.; Wolff, C.; Sanwald, K. E.; Crampton, A. S.; Ridge, C. J.; Jackel, F.; Feldmann, J.; Tschurl, M.; Heiz, U. Cluster Size Effects in the Photocatalytic Hydrogen Evolution Reaction. *J. Am. Chem. Soc.* **2013**, *135*, 13262–13265.
- (19) Yin, Y.; Han, J.; Zhang, Y.; Zhang, X.; Xu, P.; Yuan, Q.; Samad, L.; Wang, X.; Wang, Y.; Zhang, Z.; Zhang, Z.; Cao, X.; Song, B.; Jin, S. Contributions of Phase, Sulfur Vacancies, and Edges to the Hydrogen Evolution Reaction Catalytic Activity of Porous Molybdenum Disulfide Nanosheets. *J. Am. Chem. Soc.* **2016**, *138*, 7965–7972.
- (20) Feng, J.-X.; Ding, L.-X.; Ye, S.-H.; He, X.-J.; Xu, H.; Tong, Y.-X.; Li, G.-R. Co(OH)₂@PANI Hybrid Nanosheets with 3D Networks as High-Performance Electrocatalysts for Hydrogen Evolution Reaction. *Adv. Mater.* **2015**, *27*, 7051–7057.

- (21) Tian, T.; Huang, L.; Ai, L. H.; Jiang, J. Surface Anion-Rich NiS_2 Hollow Microspheres Derived from Metal—Organic Frameworks as a Robust Electrocatalyst for the Hydrogen Evolution Reaction. *J. Mater. Chem. A* **2017**, *5*, 20985–20992.
- (22) Jiang, N.; Bogoev, L.; Popova, M.; Gul, S.; Yano, J.; Sun, Y. Electrodeposited Nickel-Sulfide Films as Competent Hydrogen Evolution Catalysts in Neutral Water. *J. Mater. Chem. A* **2014**, 2, 19407–19414.
- (23) Jiang, N.; Tang, Q.; Sheng, M.; You, B.; Jiang, D.-e.; Sun, Y. Nickel Sulfides for Electrocatalytic Hydrogen Evolution under Alkaline Conditions: A Case Study of Crystalline NiS, NiS₂, and Ni₃S₂ Nanoparticles. *Catal. Sci. Technol.* **2016**, *6*, 1077–1084.
- (24) Jiang, N.; You, B.; Sheng, M.; Sun, Y. Bifunctionality and Mechanism of Electrodeposited Nickel-Phosphorous Films for Efficient Overall Water Splitting. *ChemCatChem* **2016**, *8*, 106–112.
- (25) Luo, J.; Im, J. H.; Mayer, M. T.; Schreier, M.; Nazeeruddin, M. K.; Park, N. G.; Tilley, S. D.; Fan, H.; Gratzel, M. Water Photolysis at 12.3% Efficiency via Perovskite Photovoltaics and Earth—Abundant Catalysts. *Science* **2014**, 345, 1593—1596.
- (26) Stern, L. A.; Feng, L.; Song, F.; Hu, X. Ni₂P as a Janus Catalyst for Water Splitting: the Oxygen Evolution Activity of Ni₂P Nanoparticles. *Energy Environ. Sci.* **2015**, *8*, 2347–2351.
- (27) You, B.; Liu, X.; Hu, G.; Gul, S.; Yano, J.; Jiang, D.-e.; Sun, Y. Universal Surface Engineering of Transition Metals for Superior Electrocatalytic Hydrogen Evolution in Neutral Water. *J. Am. Chem. Soc.* **2017**, *139*, 12283–12290.
- (28) Liu, C.; Colón, B. C.; Ziesack, M.; Silver, P. A.; Nocera, D. G. Water Splitting–Biosynthetic System with CO₂ Reduction Efficiencies Exceeding Photosynthesis. *Science* **2016**, 352, 1210–1213.
- (29) Peng, Z.; Jia, D.; Al-Enizi, A. M.; Elzatahry, A. A.; Zheng, G. From Water Oxidation to Reduction: Homologous Ni–Co Based Nanowires as Complementary Water Splitting Electrocatalysts. *Adv. Energy Mater.* **2015**, *5*, 1402031.
- (30) Nichols, E. M.; Gallagher, J. J.; Liu, C.; Su, Y.; Resasco, J.; Yu, Y.; Sun, Y.; Yang, P.; Chang, M. C. Y.; Chang, C. J. Hybrid Bioinorganic Approach to Solar—to—Chemical Conversion. *Proc. Natl. Acad. Sci. U. S. A.* **2015**, *112*, 11461—11466.
- (31) Tran, P. D.; Tran, T. V.; Orio, M.; Torelli, S.; Truong, Q. D.; Nayuki, K.; Sasaki, Y.; Chiam, S. Y.; Yi, R.; Honma, I.; Barber, J.; Artero, V. Coordination Polymer Structure and Revisited Hydrogen Evolution Catalytic Mechanism for Amorphous Molybdenum Sulfide. *Nat. Mater.* **2016**, *15*, 640–646.
- (32) Torella, J. P.; Gagliardi, C. J.; Chen, J. S.; Bediako, D. K.; Colon, B.; Way, J. C.; Silver, P. A.; Nocera, D. G. Efficient Solar–to–Fuels Production from a Hybrid Microbial–Water–Splitting Catalyst System. *Proc. Natl. Acad. Sci. U. S. A.* **2015**, *112*, 2337–2342.
- (33) Miao, J.; Xiao, F. X.; Yang, H. B.; Khoo, S. Y.; Chen, J.; Fan, Z.; Hsu, Y. Y.; Chen, H. M.; Zhang, H.; Liu, B. Hierarchical Ni–Mo–S Nanosheets on Carbon Fiber Cloth: A Flexible Electrode for Efficient Hydrogen Generation in Neutral Electrolyte. *Sci. Adv.* **2015**, *1*, e1500259.
- (34) Kang, D.; Kim, T. W.; Kubota, S. R.; Cardiel, A. C.; Cha, H. G.; Choi, K. Electrochemical Synthesis of Photoelectrodes and Catalysts for Use in Solar Water Splitting. *Chem. Rev.* **2015**, *115*, 12839–12887.